Hydrogen atom-ion synergy in surface lattice modification at sub-threshold energy

L. Gao[1‡*], M. Wilde[2‡], A. Manhard[1], U. von Toussaint[1] and W. Jacob[1]

[1]Max-Planck-Institut für Plasmaphysik, Boltzmannstr. 2, 85748 Garching, Germany

[2]Institute of Industrial Science, University of Tokyo, Komaba 4-6-1, Meguro-ku, 153-8505 Tokyo, Japan

[‡]Authors with the same contribution to the present work

[*]E-mail address: liang.gao@ipp.mpg.de

Abstract Low-energy hydrogen-isotope (HI) plasma is widely applied for industrial surface processing. Here we demonstrate that HI plasma - even with ion energies far below the threshold for stable Frenkel pair production - can strongly modify crystalline materials by forming heavily lattice-distorted surface layers with a thickness of several nanometers and a HI content of several atomic percent. We experimentally reproduce the identical lattice modification at deuterium and hydrogen plasma-irradiated tungsten (W) surfaces when the sub-threshold HI ion energies are adjusted such as to transfer equal amounts of kinetic energy in collisions with W lattice atoms. A physical model for the low-energy generation of primary defects is proposed, which involves the synergy between temporary Frenkel pair creation by sub-threshold HI ion collisions and vacancy stabilization by trapping of solute HI atoms. Such synergistic defect generation is generally expected upon injection of energetic projectiles (ions, neutrons) into HI-containing solids and likely contributes to material degradation. As a means of surface modification, the fabrication of nanometer-scale hydrogen-rich surface layers on materials (even those with negligible hydrogen solubility) via low-energy H plasma exposure promises utilization potential in catalysis and electrochemistry.

Keywords: Plasma-Surface Interaction; Radiation damage, Displacement threshold; Solute hydrogen; Synergy

Published in:	Acta Materialia, **201** (2020) 55–62.
doi:	10.1016/j.actamat.2020.09.065
Submitted:	11.04.2020
Accepted:	15.09.2020
Available online:	23.09.2020

Introduction

Atomic hydrogen (H) is highly reactive and a ubiquitous impurity in many materials, where it modifies their electronic and mechanical properties through interactions with lattice atoms and/or crystal defects. Extensively investigated hydrogen-defect interactions [1,2] affect important applications of hydrogen such as plasma processing [3,4] and electrical passivation of semiconductor devices [5,6], and may cause adverse effects such as hydrogen embrittlement [7, 8]. In particular the retention of the expensive and radioactive tritium (T) isotope due to trapping at irradiation-induced defects in plasma-facing materials (e.g., tungsten (W), steels, etc.) poses greatest cost and safety concerns for thermonuclear fusion reactors [9,10]. Therefore, the mechanisms of defect creation under hydrogen plasma irradiation must be thoroughly understood. However, the theoretically predicted [11-14] influence of lattice-dissolved (solute) hydrogen on the production of defects under energetic particle irradiation has remained largely unexplored. One reason for this is the difficulty to experimentally assess solute hydrogen, which exists in non-H-dissolving materials with often unmeasurably small concentrations and is only metastable even under non-equilibrium hydrogen loading conditions, such as cathodic charging and plasma or ion irradiation. On the other hand, the H concentration underneath hydrogen plasma-irradiated solid surfaces can be estimated theoretically with a model [15,16] that considers the steady-state balance between the implantation-, the reemission- and the permeation fluxes of plasma particles [17,18]. This 1-dimensional flux-balance model [17-19] shows that substantial H concentrations (up to H/W = 10^{-3}) can build up beneath plasma-exposed tungsten (W) surfaces [18,19]. This solute H, however, is unstable against out-diffusion and desorption when the ion irradiation stops because the H solubility in pristine W is extremely low (H/W = 10^{-18} in 1 bar H_2 at 298 K) due to a strongly endothermic solution enthalpy (1.04 eV/H) [20, 21]. All stably retained hydrogen detectable after the plasma exposure is trapped at crystal defects. Here, irradiation-induced damage far exceeds the intrinsic defect density and ultimately dominates the hydrogen content [22,23].

The present work thus investigates the role of solute hydrogen isotope (HI) atoms in the severe lattice modification that occurs on W surfaces under HI plasma irradiation even at ion energies far below the threshold for stable Frenkel pair production [24]. The impact of HI ions (M_1) with sufficient incident energy (E_0) can displace W atoms (M_2) from their lattice sites, creating vacancies and nearby interstitial W atoms (Frenkel pairs). This collision process has been investigated both experimentally [25,26] and computationally [27-30]. Conservation of energy and momentum defines the kinetic energy transferred to the W atoms (E_2) as:

$$E_2 = \frac{4M_1 \cdot M_2 \cdot E_0}{(M_1+M_2)^2} sin^2 \frac{\theta}{2} \qquad (1)$$

where θ is the center of mass scattering angle. If E_2 exceeds the so-called kinetic displacement energy threshold, the displaced interstitial W atom will be sufficiently far away from the vacancy so that the Frenkel pair is stable against prompt recombination. For W, this threshold is 40-70 eV [24] depending on the grain orientation, thus creation of stable Frenkel pairs requires an incident deuterium (D) ion energy of at least 930 eV (Eq. (1)). Recently, however, a severely lattice-distorted layer was discovered on polycrystalline W surfaces after exposure to D plasma with an ion energy of only 215 eV (Fig. 1 (b) and Fig. 5 in Ref. [19]). The 10 nm thick modified layer contained a

uniformly distributed D concentration of D/W ~10^{-1}, which is the highest reported value for a non-hydride-forming metal after plasma irradiation with sub-threshold ion energy. The distorted layer was accordingly addressed as 'deuterium supersaturated surface layer' (DSSL). Importantly, the distortion effect shows an onset in the incident D ion energy at 115 eV [19], which corresponds to a maximum energy transfer to W atoms of merely 5 eV (Eq. (1), $\theta = 180°$). Evidently, elastic collision kinematics (Eq. 1) alone cannot explain the DSSL formation so far below the kinetic displacement threshold.

Taking the prediction [11-14] further that solute D atoms (i.e., D plasma ions thermalized after implantation into the W lattice) can participate in defect creation processes [19], the present work proposes a physical model for the mechanism that leads to formation of HI-SSLs on plasma-exposed materials through the synergy of low-energy HI ions and solute HI atoms, which generate and stabilize defects, respectively. Based on our present experimental results (detailed below) and previous findings [11-14] we suggest that the sub-threshold collisions with HI ions create temporary Frenkel pairs, which are unstable against recombination in absence of solute HI atoms. When solute HIs are abundant, however, trapping of nearby HI atoms in the vacancies is considered to reduce the recombination rate of Frenkel pairs, thereby stabilizing the defects. This synergistic mechanism of defect generation by sub-threshold HI ions and stabilization by solute HI atoms is expected to apply universally, for all hydrogen isotopes (H, D and T), as well as in any crystalline host material under HI plasma irradiation. To experimentally validate the above-proposed synergistic defect generation scenario we here apply scanning electron microscopy (SEM) and H- and D-specific depth profiling with nuclear reaction analysis (NRA) to demonstrate that H/D plasma irradiation produces H/D-SSLs of identical morphology, thickness, and HI content on W surfaces if – under otherwise identical conditions – the HI ion energy is adjusted such that equivalent amounts of kinetic energy are transferred in the primary collisions with W lattice atoms. According to Eq. (1), H ions transfer the same kinetic energy to W atoms as D ions ($E_2 \propto \approx M_1 E_0$) if they impact with approximately twice ($M_D/M_H \approx 2$) the energy of the incident D ions. The surface morphology at identical locations of each sample before and after the H/D plasma exposure was characterized by SEM. The H and D depth distributions in the SSLs formed on the plasma-exposed samples were measured quantitatively with ^{15}N-^{1}H [31,32] and a high-resolution variant of ^{3}He-^{2}D [19] NRA, respectively.

1. Experimental

2.1 Plasma exposure

Polycrystalline, hot-rolled W samples (15×12×0.8 mm^3, 99.97 wt. % purity, Plansee SE, Austria), with grain sizes in the order of 1 μm [33], were chemo-mechanically polished to a mirror-finish and annealed in vacuum at 1200 K for 2 hours. Before exposure to hydrogen isotope (HI) plasma, the surface morphology of all samples was characterized with SEM (FEI HELIOS NanoLab 600) with up to ~10 nm lateral resolution and 30 kV maximum acceleration voltage. A set of T-shaped markers was applied to the samples using FIB cutting [34] prior to annealing. This allowed for the identification of identical positions on the samples before and after HI plasma exposure.

HI plasma exposures were performed in a low-temperature electron cyclotron resonance plasma source, PlaQ [35]. To ensure that equivalent amounts of kinetic energy are transferred in the primary collisions with W lattice atoms (Eq. (1)), we exposed the W samples to H plasma at a DC bias voltage of 400 V and to D plasma at 200 V. Including the added plasma potential of 15 eV [35], the corresponding ion energies were 415 and 215 eV, respectively. The ion flux from the plasma is composed of different ion species (H_3^+/D_3^+, 94 %, H_2^+/D_2^+, 3 % and H/D^+, 3 %). Only the minority atomic ions (H^+/D^+) carry the full ion energy and thereby contribute to sub-threshold temporary Frenkel pair generation by exceeding the empirical energy transfer threshold (115 eV/D or 230 eV/H, Eq. (1)). Hence, only 1 % of the total applied H/D particle fluence is actually responsible for the SSL formation (a D_3^+ ion contributes 3 D atoms to the total D particle fluence). All other experimental parameters, including ion flux (10^{20} $m^{-2}\cdot s^{-1}$), particle fluence (6×10^{24} m^{-2}), sample temperature (300 K) and W material grade, were identical.

2.2 Nuclear reaction analysis

The quantitative H and D depth distributions in the SSLs formed on the plasma-exposed W samples were measured with NRA. ^{1}H depth profiles were obtained through $^1H(^{15}N,\alpha\gamma)^{12}C$ NRA using normal-incidence $^{15}N^{2+}$ ion beams of 10-30 nA (provided by the MALT tandem accelerator at the University of Tokyo) near the narrow 6.385 MeV energy resonance (E_{res}) of the $^1H(^{15}N,\alpha\gamma)^{12}C$ reaction [31,32]. The γ-ray yield from the nuclear reaction normalized to the number of incident ^{15}N ions (Y) is proportional to the H concentration ([H]) at a probing depth d, which is selected by the incident ^{15}N ion energy (E_i) as $d = (E_i - E_{res})/S$, where S is the stopping power (S) of the sample material for the ~6.4-MeV ^{15}N ions. For H quantitation [32], the γ-detection efficiency was calibrated with Kapton ($(C_{22}H_{10}O_5N_2)_n$) foil as H-concentration standard (density: 1.45 g/cm^3, H-content: 2.284×10^{22} cm^{-3}, and S = 1.288 keV/nm), establishing the relation [H] (cm^{-3}) = Y (cts/μC) × S (keV/nm) / α, where $\alpha = 1.302\times10^{-19}$. The stopping power of materials with significant H content in the matrix increases according to Bragg's rule [31]. For the HSSL that includes 9.3 at. % of H (Fig. 2), the stopping power of pure W (S = 4.010 keV/nm) increases by 0.7 % to S = 4.038 keV/nm.

The D depth profiles were measured with $^2D(^3He,p)^4He$ NRA [19] at 690 keV beam energy at the tandem accelerator in IPP Garching, Germany. Both the emitted protons and ^{4}He particles were detected. The best resolution achievable by detecting the emitted ^{4}He particles is 16 nm, which is comparable to the thickness of the SSL and hence not sufficient to analyze the D depth distribution in the DSSL. To resolve the latter, we combined ^{3}He NRA with argon sputtering [19]. By sputtering small increments of material from the sample surface with a 200-eV Ar plasma followed by ^{3}He NRA measurements of the remaining D content, the depth resolution was enhanced to 3 nm. Hence, the depth resolution is determined by the thickness removed during each sputtering step [19]. In principle, this technique allows for even further enhancement of the depth resolution by using smaller Ar-sputtering steps.

2. Results

3.1 Surface modification

Fig. 1 shows the surface morphologies of the W samples before and after H/D plasma exposure. The plasma-exposed surfaces appear coarse due to SSL formation [19]. The morphological features on the DSSL and HSSL samples are virtually identical (see also Fig. S1 in the *Supplementary Materials*). The defect structures in the post-exposure SEM images are small compared with the W grains. Single vacancies are too small be visualized by SEM, hence the observed structures are considered to be secondary features produced by clustering of primary defects, i.e., of stabilized single vacancies. The coarse structures in the SEM images of the SSL-modified W surfaces only appear in backscattering contrast and are hence not simply due to surface roughness, but must be caused by the defect microstructure inside the SSL volume. Presently, the detailed microstructure of these visible defects is still unknown. SEM images of an electron-transparent W sample [36] show a very high defect density after the plasma exposure of 6×10^{24} D·m^{-2} (see Fig. S2 in the *Supplementary Materials*), which precludes identifying any individual structures. Experiments with lower particle fluence may be able to characterize individual defects in the initial stage of SSL formation. We note in passing that additional implantation experiments and SDTrimSP simulations confirm that SSL formation is not related to Ar ions or typical plasma impurity species (C, N, O…), as their penetration depths (< 2 nm) are much shallower than those of HI ions and can therefore not account for the observed SSL thickness of ~ 10 nm (see Fig. S3 in *Supplementary Materials*).

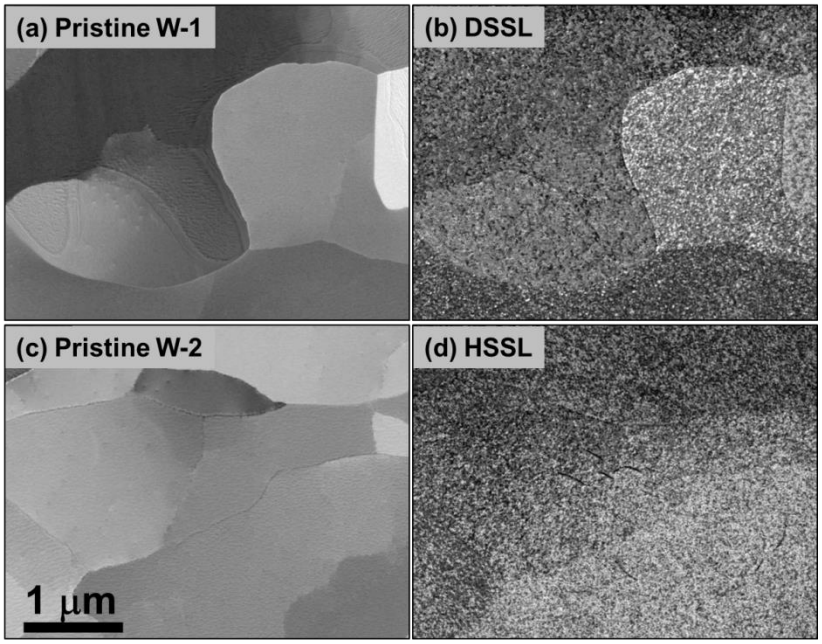

Figure 1. Surface morphologies of polycrystalline W samples before (i.e., pristine W surfaces in (a) & (c)) and after H/D plasma exposure (i.e., with H/D-supersaturated surface layers in (b) & (d) for the same area as in (a) & (c), respectively). All SEM images share the same scale bar shown in (c).

3.2 H/D depth profiles

Fig. 2 shows the comparison of ^{15}N NRA γ-yield curves from a pristine W sample and a 415-eV H plasma-irradiated W sample (i.e., with a HSSL). Both profiles exhibit a peak at the resonance energy (E_{res}), which is due to H adsorbed on the W surface. Whereas the H profile of the HSSL sample extends into ~10 nm depth as described in detail below, the pristine W profile exhibits only the surface peak and an empty W bulk, i.e., the H concentration in the pristine W is below the NRA detection limit (< 3×10^{19} cm^{-3}), as one would expect from the low H solubility and small defect densities in pristine W. From the integrated intensity of the surface peak, the H surface coverage can be quantified [32] to amount to $(2.74 \pm 0.26) \times 10^{15}$ cm^{-2}. The (full) width of the surface peak (primarily caused by vibrational Doppler-broadening [32]) is seen to extend into a depth of ~3 nm, which limits the NRA depth resolution near the surface.

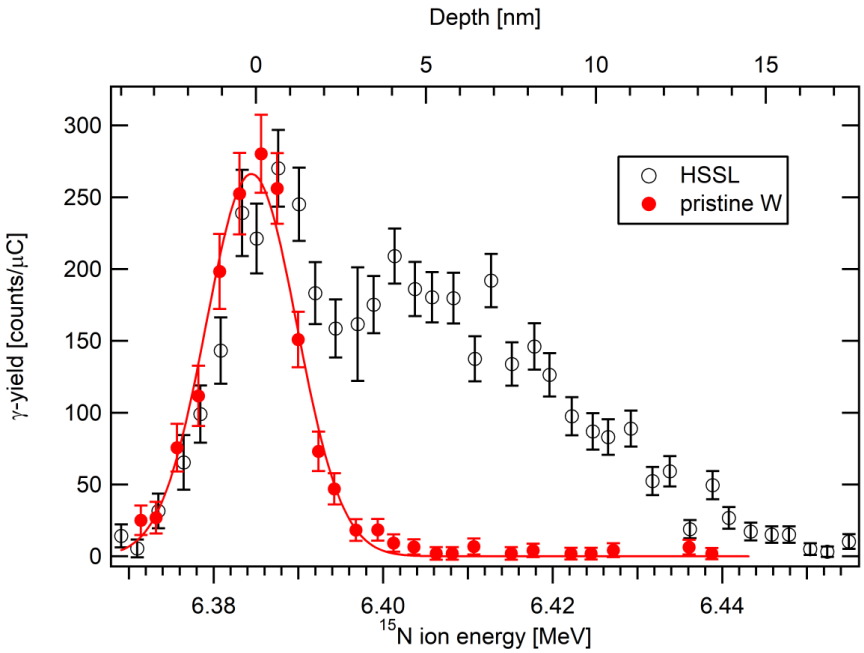

Figure 2. Comparison of ^{15}N NRA measurements of H profiles from a pristine and a hydrogen-plasma irradiated W sample, i.e., after HSSL formation.

The ^{15}N NRA γ-yield curve ('H depth profile') from the HSSL sample is shown in Fig. 3. The γ-yield is nearly constant in the topmost 6 nm at an average level of 192 ± 22 cts/μC, which corresponds to a H concentration of $(5.9 \pm 0.7)\times 10^{21}$ cm^{-3} in the plasma-modified surface layer, i.e. to a H/W ratio of 9.3 ± 1.1 at. %. Beyond ~6 nm depth, the γ-yield gradually declines to the detection limit. The ^{15}N NRA depth resolution is ~3 nm at the surface (see Fig. 2) but deteriorates at increasing depth due to ^{15}N ion energy straggling [32], which blurs the falling edge of the profile so that the region of 6-9 nm appears already H-depleted whereas surplus γ-yield is detected in depths larger than the actual H distribution. The actual H distribution is very similar to that of D as described below. The thickness of the HSSL can be judged from the inflection point in the declining edge of the γ-yield profile. A sigmoid fit to the data (blue line) locates this point in a depth of 9.5 ± 0.2 nm. Three data points of about 250 cts/μC in ~1 nm depth originate from H on the sample surface (cf. Fig. 2) and were excluded from the fit.

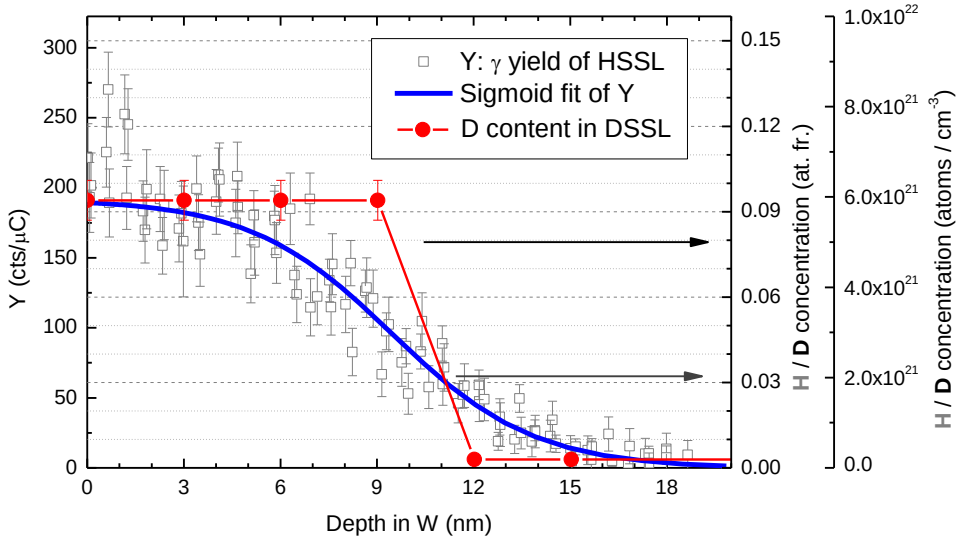

Figure 3. Depth profiles of H and D in the supersaturated surface layers on W samples formed under exposure to 415-eV H and 215-eV D plasma.

The D profile from the 215-eV D-irradiated sample obtained through ^{3}He NRA combined with Ar sputtering is plotted in filled symbols in Fig. 3. The DSSL disappears between 9 and 12 nm (the depth resolution in this experiment was only 3 nm). A refined analysis [19] revealed a uniform D distribution throughout the layer of 10.4 ± 0.4 nm thickness and a D density of (5.9 ± 0.4) ×10^{21} cm^{-3} (i.e., D/W = 9.4 ± 0.7 at. %). Hence, both SSLs formed under 415-eV H^+ and 215-eV D^+ irradiation show a thickness of about 10 nm and a retained H/D atomic fraction in the order of 10^{-1}. Together with the virtually identical H/DSSL morphologies (Fig. 1), the close resemblance of the depth distributions of H and D in the SSLs thus strongly supports our assumption that the SSL-forming modification of the H/D plasma-irradiated W surfaces follows a common physical mechanism that scales with the collisional energy transfer to the W atoms. The identical H/D depth profiles obtained by independent NRA methods clearly demonstrate also that there is no significant distortion of the D depth distribution measured by ^{3}He NRA in combination with Ar sputtering [19], as no such ion bombardment is applied prior to ^{15}N NRA for H profiling.

3.3 SDTrimSP simulation

To demonstrate consistency with our proposed mechanism, we elucidate the depth region in W that is potentially affected by the synergistic defect generation under H plasma irradiation with the aid of SDTrimSP simulations [37,38], which model the transport of energetic H ions in the W matrix as a series of binary collisions described by kinematics as in Eq. (1). This reveals how the probability for H-W collisions that transfer more energy than the empirical SSL formation threshold of 5 eV to W lattice atoms [19] varies as a function of depth underneath the W surface and is shown by open symbols in Fig. 4 for H^+ plasma ions impacting on W with 415 eV of initial energy. In the synergistic modification mechanism, the formation of stabilized vacancies depends on both the kinetic collisions (i.e., the creation of temporary Frenkel pairs) and on the trapping of nearby solute H atoms that can stabilize the created vacancies. The concentration profile of solute H atoms (filled symbols in Fig. 4) is determined by the

majority of the impinging hydrogen ions (97% of the plasma flux is H_3^+ with 138 eV per H, see Section 2.1) and was calculated in the 1-d flux balance model [17-19]. Finally, the probability for forming a stabilized vacancy (SVFP, defined as the product of the temporary Frenkel pair creation probability and the solute H concentration) is plotted as the bold line in Fig. 4. It is seen that the HSSL thickness is dominated by the > 5 eV H-W collision probability depth distribution. A cutoff probability of 10^{-5} – only one collision from 50,000 projectiles occurs at the relevant depth with transferrable energy above 5 eV – results in an about 10-nm deep modified layer. This closely agrees with the observed HSSL thickness (see ^{1}H depth profile in Fig. 3). An analogous SDTrimSP simulation of 215-eV D implantation into W shows equally good agreement of the SVFP distribution with the D depth profile in Fig. 3 (Fig. S4, *Supplementary Materials*). Since the experimental H/D profiles shown in Fig. 3 appear rather flat within the SSL thickness whereas the SVFP varies strongly with depth (Fig. 4), we presume that the measured H/D distributions in the SSLs represent a saturation of H/D trapping at accumulated and agglomerated defects.

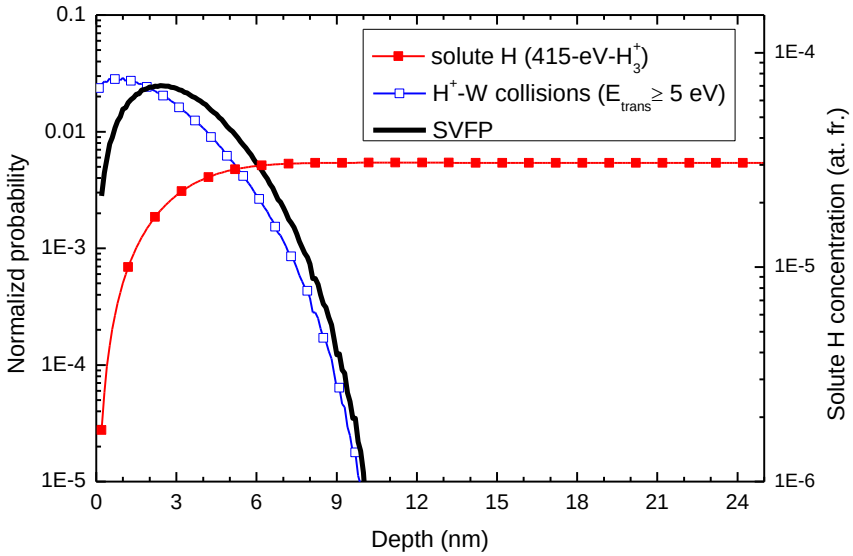

Figure 4. SDTrimSP simulation for the impact of 50,000 hydrogen plasma ions with an incident energy of 415 eV on bulk W. The 'H$^+$-W collision profile' is the probability distribution for H$^+$-W collisions with a transferred energy equal or higher than 5 eV. 'Solute H' represents the steady-state concentration profile of solute H atoms during the applied irradiation (see Eq. (2)). The stabilized vacancy formation probability (SVFP) is the product of the former two distributions. It is normalized such that the integral over depth equals unity.

3. Discussion

The empirically observed energy threshold for SSL formation under HI plasma irradiation of 5 eV [19] is much smaller than the kinetic displacement energy threshold for stable Frenkel pair creation in a H-free W matrix (40-70 eV) [24], which highlights the crucial role of solute HI atoms in the defect generation process. While the formation of the defect-rich layer by HI ions with energies far below the kinetic displacement threshold energy is highly reproducible and has been observed in numerous follow-up experiments (see Fig. 5 below), an atomistic description of the phenomenon is still lacking. We thus aim here to provide a first explanation for the generation of primary, atomic-level type defects (Frenkel pairs) in sub-threshold HI ion collisions with W lattice atoms in the presence of solute HIs, which represent the underlying elementary

events that, ultimately, cause SSL formation. Note that the agglomeration of such primary defects into larger structures which give rise to the final SSL microstructure and trapped H/D contents observed by SEM and NRA, respectively, is not included in our consideration as we do not yet have information on the nature of the defect agglomeration process and what determines the final H/D concentrations in the saturation state. From the mechanistic viewpoint at the atomic level, one conceivable role of solute HI atoms may be to enhance the production rate of temporary vacancies under low-energy HI ion impact, e.g. by lowering the kinetic energy barrier height for collisional Frenkel pair creation. Such a reduction of the kinetic barrier height may result from the local strain introduced by the volumetric contribution of HI atoms to the matrix (lattice expansion by HI [11]), which enlarges the distance and reduces the cohesion between W lattice atoms [12, 13]. Another possibility is that the solute HI atoms may block the recombination of the temporary Frenkel pairs by trapping in the vacancy or by binding to the interstitial W atom. Also the latter can act as a trapping site for solute HI atoms as suggested by recent DFT calculations [14]. Our model focuses on this latter scenario, in which trapping of solute HI atoms at either the vacancy or the interstitial atom is expected to largely suppress the recombination rate of temporary Frenkel pairs.

To stabilize a temporary Frenkel defect, a nearby solute HI atom has to bind into the vacancy (or to the interstitial W atom) before the Frenkel pair recombines. The time scale of this process is determined by the HI atom mobility in the lattice and the distance between the HI atom and the created temporary defect. The latter is determined by the solute HI concentration and the former depends mainly on the sample temperature (i.e., HI lattice site hopping frequency). According to the 1-dimensional flux-balance model [17-19], the maximum concentration of solute HI atoms at the mean implantation depth (r_{impl}, ~5 nm under the applied conditions) extends nearly flat into larger depth (~ 1 μm) [18] during irradiation (Fig. 3) and is expressed as:

$$C_{max}^{HI} \approx \frac{r_{impl} \times \Gamma_{impl}}{\rho_W \times D(T)} \qquad (2)$$

where ρ_W is the atomic density of W, D(T) the HI diffusion coefficient at temperature T, and $\Gamma_{impl} = \Gamma_{incident} - \Gamma_{reflection}$, the difference between the incident particle flux $\Gamma_{incident}$ and the reflection yield $\Gamma_{reflection}$. The probability for HI trapping at a created temporary W vacancy or interstitial atom (trapping probability, TP) is proportional to the flux of passing-by solute HI atoms, which can be described by the product between the local concentration of solute HI atoms (C_{local}^{HI}) at the site of a created temporary Frenkel defect and the HI mobility. In the SSL-affected depth region (~10 nm), C_{local}^{HI} decreases linearly from C_{max}^{HI} *at* r_{impl} (about 5 nm) towards the surface, where it becomes zero (see Fig. 1 in Ref. [18]) but has a similar dependence on $\Gamma_{incident}$ and T as C_{max}^{HI}. Thus, as an important practical insight, SSL formation cannot be prohibited by elevated temperatures during exposure to a given particle flux within the thermal stability limits of HI trapping in vacancies [39-41], because at elevated temperatures also the HI mobility increases.

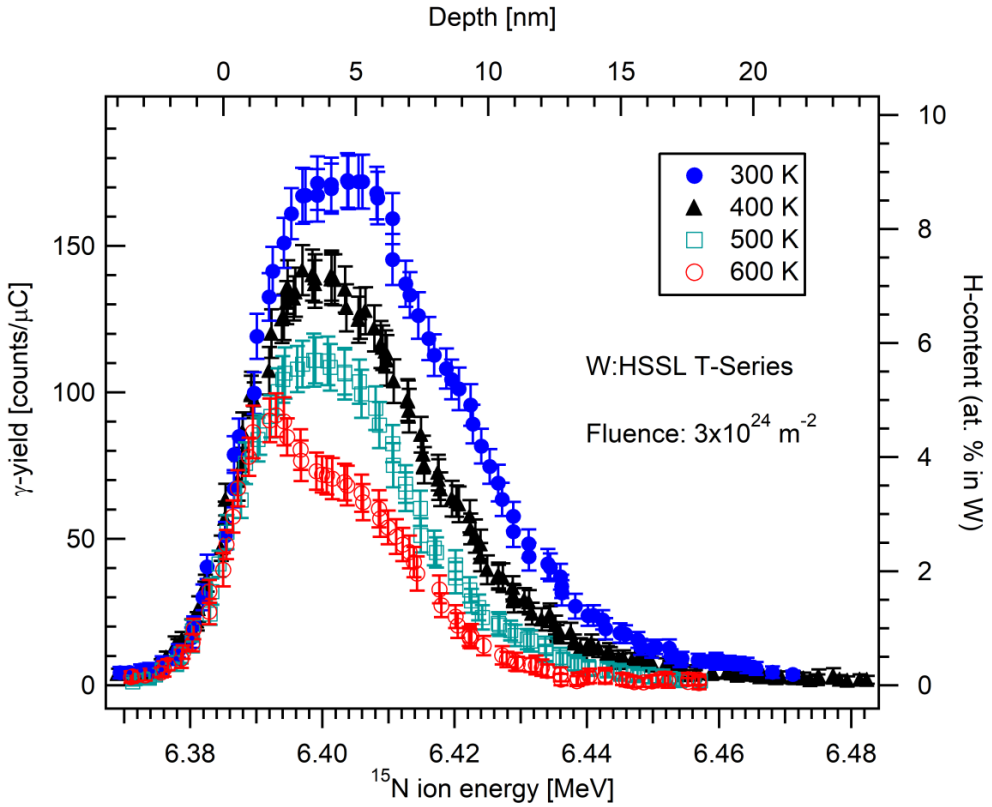

Figure 5: ^{15}N NRA H depth profiles in SSLs formed at sample temperatures from 300 to 600 K on 415-eV H plasma-exposed W.

To demonstrate this prediction, we performed both 415-eV H- and 215-eV D-plasma exposures at different temperatures under otherwise identical conditions. The ^{15}N NRA H profiles obtained from the W surfaces exposed to 415-eV H plasma between 300 and 600 K shown in Fig. 5 clearly indicate that a HSSL forms at temperatures up to 600 K. In all cases the appearance of massive lattice defects in the SSL volume is also evident in backscattering electron contrast SEM images (see e.g., Fig. S5, Supplementary Materials). Although the trapped H concentration and the HSSL thickness in Fig. 5 decrease with increasing irradiation temperature, the H concentration retained in the SSL at 600 K still reaches ~5 at.% . These temperature-dependent changes of the H profiles may partially be explained by thermal de-trapping of H from the defects inside the HSSL. It is also quite possible that the temperature affects the defect agglomeration process that we still have to clarify, as stated before. We prefer to leave these interesting aspects for a future publication. For W [20], $D(T) = D_0 \cdot \exp[-0.39/k_B T]$ with $D_0 = 2.9\times10^{-7}$ m^{2}s^{-1} and k_B the Boltzmann constant, i.e., the solute D concentration (D/W = 10^{-8} from Eq. (2) under our exposure conditions) is 3 orders of magnitude smaller at 600 K than at 300 K (D/W = 10^{-5}) [18,19], yet evidently SSL formation, i.e., Frenkel pair creation and HI-stabilization, still occurs at this temperature. Further increasing the irradiation temperature until created vacancies can no longer stably trap solute HI atoms may suppress or even prevent SSL formation. Experimental de-trapping energies of D from vacancies or their clusters in W [39] agree well with theoretical predictions [40,41] and correspond to D release between ~500 and ~850 K [39]. Hence plasma irradiations at temperatures above 900 K should suppress HI trapping in vacancies thereby preventing SSL formation. At present, verification of the latter expectation is experimentally challenging, however, as the maximally achievable temperature in our plasma source [35] is 600 K.

In our proposed mechanism for lattice modification under HI plasma irradiation at sub-threshold ion energies, the stabilization of temporary Frenkel pairs via trapping of HI atoms plays a critical role. This poses the pertinent question whether a similar SSL formation as observed here for HI plasma-exposed W might also occur on He-irradiated W surfaces. Although at much lower concentration that the HIs (D, T), He is an inevitable component in fusion plasmas, and as an implanted impurity in W lattices He interacts even more strongly with vacancy defects (interaction energy ~ 4 eV) [42] than HIs (≤~1.5 eV [39-41]). In principle, stabilization of temporary vacancies by implanted He and a potential synergistic formation of a He-SSL might therefore also be expected to occur on W surfaces under He plasma irradiation. In fact, the low-energy formation of surface vacancies and adatoms (e.g., Frenkel pairs) has been observed in molecular dynamics simulations of He-implanted W [43], and a modified trap mutation process that can occur within a few atomic layers of a W surface to produce a Frenkel pair (again in the form of a near surface vacancy and a tungsten adatom) has been reported [44]. These processes seem to bear some resemblance with our proposed synergistic defect generation mechanism by HIs, although they are limited to a region in much closer vicinity of the surface.

On the other hand, the possibility to observe an SSL depends also on other factors such as the kinetic collisions and ion penetration (stopping). The decisive differences between HIs and He in this regard are the much larger penetration depth and lower sputtering yield of HI ions compared with He ions of the same energy. The presently applied energy of 215 eV for D is below the threshold for W sputtering by D (~250 eV), but already significantly above the sputtering threshold of He atoms (~110 eV). At the same ion energy, even if formed, a He-induced SSL would thus be unlikely to survive the sputtering; a problem that is further exacerbated by the abundance of He^{2+} ions (carrying twice the energy) in the plasma. Given that He ions transfer twice the energy of D to W lattice atoms according to our model (Eq. (1)), an energy window to create an SSL with He while staying below the sputtering threshold may still exist. However, in this case the expected thickness of the SSL would reduce significantly to about $1/8^{th}$ (half the energy and 2^2=4 times the stopping) of the HI-induced SSL, i.e., to about 1 nm, which again implies increased susceptibility to sputtering by impurities and He^{2+}. It should thus be very challenging to experimentally resolve a He-distorted layer, which we would expect to be extremely thin. These arguments equally apply to all other elements heavier than hydrogen and thereby emphasize the likely unique ability of HI plasmas to create SSLs on material surfaces. Moreover, regarding trap mutation under He irradiation, we note that the strong self-trapping binding energies of He atoms [45] can even exceed those between He and primary vacancies [42]. He atoms may thus be preferentially absorbed by He-clusters rather than by a newly collision-created vacancy. Hence, the probability of vacancy stabilization by He may be even lower than that on HI-irradiated W surfaces under comparable irradiation conditions.

Having pointed out the probably unique ability of HI plasmas to create SSLs on W surfaces by synergistic Frenkel pair creation, we note that also other types of defects can be produced in the W matrix during HI plasma exposure, such as dislocations [46,47] and cracking [17,36,48]. There still exists a gap in our model between the generation of primary Frenkel pairs and the evolution of the microstructure that is eventually observed as SSL after agglomeration of the atomic defects, so it is possible that other defect types contribute to SSL formation. Taking dislocations as an example, we note that the generation mechanism of dislocations under HI plasma irradiation [46] is very different from that of an SSL. Firstly, SSL formation involves kinetic collisions.

These are not at all relevant for dislocation generation, which takes place in depths far beyond the implantation zone during the irradiation [46]. Hence, a critical ion energy (threshold) is observed for DSSL creation [19] but not for D-induced dislocation production in W [47]. Moreover, the stresses induced by ion implantation are compressive within but tensile beyond the implantation zone, which are just opposite conditions to the ones favorable for dislocation formation in larger depths [46]. Therefore, and since also the concentration of D trappd at agglomerated defects in the DSSL very largely exceeds typical dislocation densities, it appears questionable whether dislocations play an important role in SSL formation.

We would finally like to emphasize that our proposed mechanism of defect generation by HI atom-ion synergy is a simple, heuristic model that aims to provide a first interpretation of the SSL formation process and explains in particular the evident importance of kinetic collisions at sub-threshold energies and its reproducibility for H and D. A promising modelling path towards elucidation of the key dynamical processes would be the simulation of collision cascades in pure and hydrogenated tungsten combined with a time-dependent (TD) study of the formation and annealing of defects as a function of the primary particle energy, hydrogen concentration, and sample temperature. For sufficiently high projectile energies and sample temperatures these processes and their relative contributions should in principle be observable in simulations. However, a proper scaling towards the experimental conditions (i.e. energies below the threshold, room temperature) will most likely require accelerated Molecular Dynamics methods [49] and dedicated rare-event handling [50]. For this purpose, the MD-potentials need to be sufficiently accurate as the rates to be estimated depend exponentially on the MD-energy barriers. Thus, a dedicated MD/TDDFT-modelling approach appears feasible but still presents a formidable task that is far beyond the scope of the present work.

From a wider perspective, lattice modification by solute hydrogen atom-particle synergy has implications that reach far beyond the formation of nanometer-thin HI-supersaturated layers on HI plasma-irradiated W surfaces. The synergy effects are neither restricted to HI-plasma irradiation nor to surfaces; they may also affect deeper bulk regions as well as materials other than W. Synergistic defect generation is principally expected whenever temporary Frenkel pairs are created by sub-threshold collisions of energetic particles with lattice atoms in the presence of solute HI atoms. Such conditions exist at the end of collision cascades of high-energy projectiles (ions, neutrons) injected into materials that already contain HIs, as demonstrated by Schwarz-Selinger *et al.* [23]. Synergistic defect generation occurs also during simultaneous co-implantation of HIs with other ion species [51,52]. In both cases, stabilisation of irradiation-induced temporary vacancies by solute D at the end of the collision cascades (where the W projectile energy falls below the kinetic threshold for permanent Frenkel pair creation) explains the observed D retention enhancement. Analogous defect generation by hydrogen-neutron synergy is expected to enhance HI retention in the bulk of materials irradiated simultaneously by HI plasma and neutrons (such as in fusion reactor vessels), and may contribute to the embrittlement of uranium fuel rod cladding (consisting of H-dissolving zirconium) in nuclear fission reactors [53]. Sub-threshold hydrogen atom-ion synergy might also affect medical diagnostics [54] and material analysis [55] with proton beam techniques, as well as H plasma treatments in the semiconductor device industry [3, 4], as the incident protons may create more defects in the irradiated materials than so far anticipated.

Aside of the potentially detrimental enhanced defect generation in materials, H atom-ion synergy during low-energy HI plasma (or ion) irradiation may offer exciting perspectives to fabricate nanometer-scale HI-rich surface layers on materials that do not naturally dissolve hydrogen (such as demonstrated here for W). Such plasma-modified hydrogen-rich surface layers could have outstanding application potential in heterogeneous catalysis of hydrocarbon hydrogenation, where hydrogen below the catalyst surface is well known as a crucial reactive species [56-59] but has hitherto been exceedingly difficult to produce in metals with negligible HI solubility [57]. Here, synergistic low-energy H plasma modification may present a facile route to introduce substantial amounts (several at. %) of sub-surface hydrogen into non-Pt-group metals to produce low-cost and sustainable catalyst materials for organic hydrogenation sythesis and fuel cells [60].

4. Conclusion

In summary, we have experimentally validated a sub-threshold lattice modification process on W surfaces exposed to two different low-energy hydrogen isotope (HI) plasmas and reproduced the resulting hydrogen/deuterium depth profiles in the created SSLs by adjusting the ion energy such as to appropriate equal energy transfer to W lattice atoms in collisions with incident HI ions. We tentatively explain the observed massive creation of primary defects by HI ions implanted into W with sub-threshold ion energies by a synergy of temporary W Frenkel pair generation in collisions with HI ions and stabilization of these temporary defects by trapping of solute HI atoms. Our proposed model of hydrogen atom-ion synergy is expected to be relevant also in other systems wherever sub-threshold particle collisions with lattice atoms create temporary Frenkel pairs in presence of solute HI atoms. We strongly invite additional experiments and theory to further verify (or falsify) our model and to clarify the influence of experimental parameters such as ion flux/fluence, ion energy, and temperature on the SSL formation and to reveal the nature of the defect agglomeration process. The synergistic low-energy defect creation mechanism we propose may have wider implications for materials under simultaneous exposure to hydrogen and energetic particle irradiation, as well as application prospects as a versatile route to fabricate novel catalytic or functional materials with H-enriched surface layers.

Acknowledgements

We are grateful to Katja Hunger for help on sample preparation. Thanks are further due to Michael Fußeder and Joachim Dorner for help with the ^{3}He NRA measurements and to Hiroyuki Matsuzaki for assistance in the MALT accelerator operation for ^{15}N NRA. This work has been carried out within the framework of the EUROfusion Consortium and has received funding from the Euratom research and training program 2014-2018 and 2019-2020 under grant agreement No 633053. Work performed under EUROfusion WP PFC. The views and opinions expressed herein do not necessarily reflect those of the European Commission.

References:

[1] S.M. Myers, M.I. Baskes, H.K. Birnbaum, J.W. Corbett, G.G. DeLeo, S.K. Estreicher, E.E. Haller, P. Jena, N.M. Johnson, R. Kirchheim, S.J. Pearton, M.J. Stavola, Hydrogen interactions with defects in crystalline solids, Rev Mod Phys, 64 (1992) 559-617.

[2] A. Pundt, R. Kirchheim, HYDROGEN IN METALS: Microstructural Aspects, Ann Rev Mater Res, 36 (2006) 555-608..

[3] K. Sabat, R. Paramguru, B. Mishra, Reduction of copper oxide by low-temperature hydrogen plasma, Plasma Chem Plasma P, 36 (2016) 1111-1124.

[4] H. Zhou, M. Xu, S. Xu, L. Liu, C. Liu, L. Kwek, L. Xu, Hydrogen-plasma-induced Rapid, Low-Temperature Crystallization of μm-thick a-Si: H Films, Scientific reports, 6 (2016) 32716.

[5] J. Chevallier, M. Aucouturier, Hydrogen in crystalline semiconductors, Annu Rev Mater Sci, 18 (1988) 219-256.

[6] J.R. Ritter, K.G. Lynn, M.D. McCluskey, Iridium-related complexes in Czochralski-grown β-Ga2O3, J Appl Phys, 126 (2019) 225705.

[7] W. H. Johnson, On some remarkable changes produced in iron and steel by the action of hydrogen and acids. *Proceedings of the Royal Society of London* **23** (1875), 168-179.

[8] O. Barrera, D. Bombac, Y. Chen, T. Daff, E. Galindo-Nava, P. Gong, D. Haley, R. Horton, I. Katzarov, J. Kermode, Understanding and mitigating hydrogen embrittlement of steels: a review of experimental, modelling and design progress from atomistic to continuum, J Mater Sci, 53 (2018) 6251-6290.

[9] J. Roth, E. Tsitrone, T. Loarer, V. Philipps, S. Brezinsek, A. Loarte, G.F. Counsell, R.P. Doerner, K. Schmid, O.V. Ogorodnikova, R.A. Causey, Tritium inventory in ITER plasma-facing materials and tritium removal procedures, Plasma Phys Contr F, 50 (2008) 103001.

[10] J. Knaster, A. Moeslang, T. Muroga, Materials research for fusion, Nature Physics, 12 (2016) 424-434.

[11] K. Heinola, T. Ahlgren, Diffusion of hydrogen in bcc tungsten studied with first principle calculations, J Appl Phys, 107 (2010) 113531.

[12] S.C. Middleburgh, R.E. Voskoboinikov, M.C. Guenette, D.P. Riley, Hydrogen induced vacancy formation in tungsten, J Nucl Mater, 448 (2014) 270-275.

[13] N. Fernandez, Y. Ferro, D. Kato, Hydrogen diffusion and vacancies formation in tungsten: Density Functional Theory calculations and statistical models, Acta Mater, 94 (2015) 307-318.

[14] Y. W. You, J. J. Sun, X. S. Kong, X. B. Wu, Y. C, Xu, X. P. Wang, Q. F. Fang and C. S. Liu. Effects of self-interstitial atom on behaviors of hydrogen and helium in tungsten. Phys. Scr. 95 (2020) 075708.

[15] B. Doyle, A simple theory for maximum H inventory and release: a new transport parameter, J Nucl Mater, 111 (1982) 628-635.

[16] O.K. Brice, B.L. Doyle, Steady state hydrogen transport in solids exposed to fusion reactor plasmas: Part I: Theory, J Nucl Mater, 120 (1984) 230-244.

[17] K. Schmid. Diffusion-trapping modelling of hydrogen recycling in tungsten under ELM-like heat loads. *Phys Scripta* **T167** (2016), 014025,
Note: the equation for the diffusion length in the 3rd paragraph (page 6) is supposed to be $\frac{\Delta R_D(t)}{\Delta t} = \frac{\Gamma^{Bulk}}{C^{Trap}(T)\cdot\rho}$ *instead of* $R_D(t) = \frac{\Gamma^{Bulk}}{C^{Trap}(T)\cdot\rho}t$.

[18] L. Gao, A. Manhard, W. Jacob, U. von Toussaint, M. Balden, K. Schmid, High-flux hydrogen irradiation-induced cracking of tungsten reproduced by low-flux plasma exposure, Nucl Fusion, 59 (2019) 056023.

[19] L. Gao, W. Jacob, U.von Toussaint, A. Manhard, M. Balden, K. Schmid, T. Schwarz-Selinger, Deuterium supersaturation in low-energy plasma-loaded tungsten surfaces, Nucl Fusion, 57 (2017) 016026.

[20] R. Frauenfelder. Solution and Diffusion of Hydrogen in Tungsten. *J Vac Sci Technol* **6** (1969), 388-397.

[21] D. F. Johnson, E. A. Carter. Hydrogen in tungsten: Absorption, diffusion, vacancy trapping, and decohesion. *J Mater Res* **25** (2010), 315-327.

[22] M. Rieth, R. Doerner, A. Hasegawa, Y. Ueda, M. Wirtz, Behavior of tungsten under irradiation and plasma interaction, J Nucl Mater, 519 (2019) 334-368.

[23] T. Schwarz-Selinger, J. Bauer, S. Elgeti, S. Markelj, Influence of the presence of deuterium on displacement damage in tungsten, Nuclear Materials and Energy, 17 (2018) 228-234.

[24] F. Maury, M. Biget, P. Vajda, A. Lucasson, P. Lucasson, Frenkel pair creation and stage I recovery in W crystals irradiated near threshold, Radiation Effects, 38 (1978) 53-65.

[25] J. Grzonka, J. Smalc-Koziorowska, O. Ogorodnikova, M. Mayer, K. Kurzydłowski, Electron microscopy observations of radiation damage in irradiated and annealed tungsten, Nucl Instr Meth Phys B, 340 (2014) 27-33.

[26] X. Yi, A. Sand, D. Mason, M. Kirk, S. Roberts, K. Nordlund, S. Dudarev, Direct observation of size scaling and elastic interaction between nano-scale defects in collision cascades, Europhysics Letters, 110 (2015) 36001.

[27] K. Nordlund, J. Keinonen, M. Ghaly, R.S. Averback, Coherent displacement of atoms during ion irradiation, Nature, 398 (1999) 49.

[28] A.E. Sand, M. Aliaga, M.J. Caturla, K. Nordlund, Surface effects and statistical laws of defects in primary radiation damage: Tungsten vs. iron, EPL (Europhysics Letters), 115 (2016) 36001.

[29] L. Ventelon, F. Willaime, C.-C. Fu, M. Heran, I. Ginoux, Ab initio investigation of radiation defects in tungsten: Structure of self-interstitials and specificity of di-vacancies compared to other bcc transition metals, J Nucl Mater, 425 (2012) 16-21.

[30] K. Nordlund, S.J. Zinkle, A.E. Sand, F. Granberg, R.S. Averback, R. Stoller, T. Suzudo, L. Malerba, F. Banhart, W.J. Weber, Improving atomic displacement and replacement calculations with physically realistic damage models, Nature communications, 9 (2018) 1-8.

[31] M. Wilde, K. Fukutani.. Hydrogen detection near surfaces and shallow interfaces with resonant nuclear reaction analysis. *Surf Sci Rep* **69** (2014), 196-295

[32] M. Wilde, S. Ohno, S. Ogura, K. Fukutani, H. Matsuzaki, Quantification of hydrogen concentrations in surface and interface layers and bulk materials through depth profiling with nuclear reaction analysis, JoVE (Journal of Visualized Experiments), DOI (2016) e53452.

[33] A. Manhard, G. Matern, M. Balden, A step-by-step analysis of the polishing process for tungsten specimens, Praktische Metallographie, 50 (2013) 5-16.

[34] M. Balden, S. Lindig, A. Manhard, J.-H. You, D2 gas-filled blisters on deuterium-bombarded tungsten, J Nucl Mater, 414 (2011) 69-72.

[35] A. Manhard, T. Schwarz-Selinger, W. Jacob, Quantification of the deuterium ion fluxes from a plasma source, Plasma Sources Sci T, 20 (2011) 015010. *Note: Unfortunately, the information given in the last paragraph of this article is not correct, but the information in figures 5 and 6 is correct. The contribution of the molecular ions to the total ion flux for standard conditions is: D_3^+ = 94%, D_2^+ = 3% and D^+ = 3%. Correspondingly, the contributions to the total deuteron flux in form of ions are: 97%, 2%, and 1%.*

[36] A. Manhard, L. Gao, Blisters formed by D plasma exposure in an electron-transparent tungsten sample, Nuclear Materials and Energy, 17 (2018) 248-252.

[37] W. Eckstein, R. Dohmen, A. Mutzke, R. Schneider, SDTrimSP: A Monte-Carlo Code for Calculating Collision Phenomena in Randomized Targets, in: G. Max-Planck-Institut für Plasmaphysik (Ed.) IPP Report: IPP 12/3 (2007), Max-Planck-Institut für Plasmaphysik, 85748-Garching, Germany

[38] A. Mutzke, R. Schneider, W. Eckstein, R. Dohmen. *SDTrimSP Version 5.00* IPP Report **12/08** (2011) Max-Planck-Institut für Plasmaphysik (Hrsg.), Garching bei München http://hdl.handle.net/11858/00-001M-0000-0026-EAF9-A.

[39] M. Zibrov, S. Ryabtsev, Y. Gasparyan, A. Pisarev, Experimental determination of the deuterium binding energy with vacancies in tungsten, J Nucl Mater, 477 (2016) 292-297.

[40] K. Heinola, T. Ahlgren, K. Nordlund, J. Keinonen, Hydrogen interaction with point defects in tungsten, Phys Rev B, 82 (2010) 094102.

[41] P. Grigorev, L. Buzi, A. Bakaeva, D. Terentyev, G. De Temmerman, G. Van Oost, J. Noterdaeme, Numerical analysis of TDS spectra under high and low flux plasma exposure conditions, Phys Scripta, 2016 (2016) 014039.

[42] P.E. Lhuillier, T. Belhabib, P. Desgardin, B. Courtois, T. Sauvage, M.F. Barthe, A.L. Thomann, P. Brault, Y. Tessier, Helium retention and early stages of helium-vacancy complexes formation in low energy helium-implanted tungsten, J Nucl Mater, 433 (2013) 305-313.

[43] K.D. Hammond, B.D. Wirth, Crystal orientation effects on helium ion depth distributions and adatom formation processes in plasma-facing tungsten, J Appl Phys, 116 (2014).

[44] L. Hu, K.D. Hammond, B.D. Wirth, D. Maroudas, Dynamics of small mobile helium clusters near tungsten surfaces, Surf Sci, 626 (2014) L21-L25.

[45] W.D. Wilson, C.L. Bisson, M.I. Baskes, Self-trapping of helium in metals, Phys Rev B, 24 (1981) 5616-5624.

[46] D. Terentyev, A. Dubinko, A. Bakaeva, G. De Temmerman, Strong sub-surface plastic deformation induced by high flux plasma in tungsten, Fusion Eng Des, 124 (2017) 405-409.

[47] A. Manhard, K. Schmid, M. Balden, W. Jacob, Influence of the microstructure on the deuterium retention in tungsten, J Nucl Mater, 415 (2011) S632-S635.

[48] A. Manhard, U. von Toussaint, M. Balden, S. Elgeti, T. Schwarz-Selinger, L. Gao, S. Kapser, T. Płociński, J. Grzonka, M. Gloc, Ł. Ciupiński, Microstructure and defect analysis in the vicinity of blisters in polycrystalline tungsten, Nuclear Materials and Energy, 12 (2017) 714-719.

[49] B.P. Uberuaga, R. Smith, A.R. Cleave, G. Henkelman, R.W. Grimes, A.F. Voter and K.E. Sickafus, Dynamical simulations of radiation damage and defect mobility in MgO, PhysRevB 71 (2005) 104012.

[50] T.S. van Erp. Dynamical Rare Event Simulation Techniques for Equilibrium and Nonequilibrium Systems, Advances in Chemical Physics 151 (2012), 27-60.

[51] E. Hodille, S. Markelj, T. Schwarz-Selinger, A. Založnik, M. Pečovnik, M. Kelemen, C.

Grisolia, Stabilization of defects by the presence of hydrogen in tungsten: simultaneous W-ion damaging and D-atom exposure, Nucl Fusion, 59 (2018) 016011.

[52] S. Markelj, T. Schwarz-Selinger, M. Pečovnik, A. Založnik, M. Kelemen, I. Čadež, J. Bauer, P. Pelicon, W. Chromiński, L. Ciupinski, Displacement damage stabilization by hydrogen presence under simultaneous W ion damage and D ion exposure, Nucl Fusion, 59 (2019) 086050.

[53] A. Zieliński, S. Sobieszczyk. Hydrogen-enhanced degradation and oxide effects in zirconium alloys for nuclear applications. *Int J Hydrogen Energ* **36**(2011), 8619-8629.

[54] R. P. Johnson. Review of medical radiography and tomography with proton beams. *Rep Prog Phys* **81** (2017), 016701.

[55] M. Vadrucci, G. Bazzano, F. Borgognoni, M. Chiari, A. Mazzinghi, L. Picardi, C. Ronsivalle, C. Ruberto, F. Taccetti, A new small-footprint external-beam PIXE facility for cultural heritage applications using pulsed proton beams, Nucl Instr Meth Phys B, 406 (2017) 314-317.

[56] A. Johnson, S. Daley, A. Utz, S. Ceyer. The chemistry of bulk hydrogen: reaction of hydrogen embedded in nickel with adsorbed CH3. *Science* **257** (1992), 223-225.

[57] S. Ceyer. The unique chemistry of hydrogen beneath the surface: Catalytic hydrogenation of hydrocarbons. *Accounts Chem Res* **34** (2001) 737-744.

[58] K. M. Neyman, S. Schauermann. Hydrogen Diffusion into Palladium Nanoparticles: Pivotal Promotion by Carbon. *Angewandte Chemie International Edition* **4**, (2010) 4743-4746..

[59] S. Ohno, M. Wilde, K. Mukai, J. Yoshinobu, K. Fukutani. Mechanism of olefin hydrogenation catalysis driven by palladium-dissolved hydrogen. *The Journal of Physical Chemistry C* **120** (2016) 11481-11489.

[60] D.V. Esposito, S.T. Hunt, A.L. Stottlemyer, K.D. Dobson, B.E. McCandless, R.W. Birkmire, J.G. Chen, Low-cost hydrogen-evolution catalysts based on monolayer platinum on tungsten monocarbide substrates, Angewandte Chemie International Edition, 49 (2010) 9859-9862.